



Journal of Advanced Research in Fluid Mechanics and Thermal Sciences

Journal homepage:

https://semarakilmu.com.my/journals/index.php/fluid_mechanics_thermal_sciences/index

ISSN: 2289-7879



Effect of Matrix Permeability on a Horizontal Shale Gas Well Performance using a Fully Coupled Fluid Flow with Geomechanics Model

Tareq Mohammed Al-Shami¹, Shiferaw Regassa Jufar^{1,*}, Berihun Mamo Negash¹, Lee Jang Hyun¹, Mohammed Bashir Abdullahi¹, Sameer Al-Hajri²

¹ Department of Petroleum Engineering, Universiti Teknologi PETRONAS, Malaysia

² Petroleum Engineering Department, Khalifa University, United Arab Emirates

ARTICLE INFO

Article history:

Received 11 April 2023

Received in revised form 18 June 2023

Accepted 24 June 2023

Available online 13 July 2023

Keywords:

Shale gas; matrix permeability; horizontal well; geomechanics; reservoir simulation

ABSTRACT

Recently, hydrocarbon production from unconventional oil and gas resources has emerged. The most common unconventional oil and gas resources are found in shale formations. These shale formations are well-known for being stress-sensitive. Usually, traditional tools are used to model and study production from such formations. However, conventional modeling techniques denote rock deformation using constant rock compressibility. Such an approach is useful for studying conventional hydrocarbon resources where formation stress sensitivity is insignificant. However, when it comes to modeling stress-sensitive formations such as shale formations, it is important to include the rock deformation and its effects on the overall fluid flow in porous media. To consider the rock deformation in the fluid flow model, the coupling of fluid flow with the geomechanics model has to be used. This study utilizes a fully coupled fluid flow with a geomechanics model. In addition, shale formations are also known to have an ultra-low matrix permeability, and production usually results from hydraulic fractures that act as flow conduits. Consequently, the effect of matrix permeability on hydrocarbon production is rarely studied. This study focuses on the effect of matrix permeability on the production performance of a single horizontal well in Barnett Shale. It also focuses on the effect of matrix permeability on production performance when the geomechanics effects are coupled with the fluid flow model and decoupled. The results show that the higher the matrix permeability, the better the production performance of the well. The results also show that the higher the matrix permeability, the higher the estimated cumulative production difference between the two models (when the geomechanics effects are coupled and decoupled).

1. Introduction

Hydrocarbon remains the primary energy source for most of the world's energy needs [1-3]. Hydrocarbon can be gas or oil; its source can be conventional and unconventional [4-6]. Conventional hydrocarbon formations are usually sandstone or carbonate reservoirs, and the hydrocarbon is usually trapped with a cap rock (e.g., shale formation). Conventional oil and gas reservoirs have

* Corresponding author.

E-mail address: shiferaw.jufar@utp.edu.my

<https://doi.org/10.37934/arfmts.107.2.208224>

relatively high porosity and permeability that can make hydrocarbon extraction achieved using traditional drilling and production methods [7]. The unconventional hydrocarbon resources are usually found in tight sandstone or shale formations. Those formations are well known for having extremely low permeability, which makes hydrocarbon extraction challenging [8-10]. However, with the development of technology, such as long horizontal wells and multistage hydraulic fracturing, production from such formations became viable [11-14]. As a result, production from unconventional hydrocarbon resources, especially shale formations, increased notably in recent years [15-18].

Reservoir simulators are used to numerically study the fluid flow in the reservoir for many purposes, including optimizing reservoir management and production performance. However, the conventional reservoir simulators currently used for such studies utilize constant rock compressibility to denote rock deformation. This assumption can be valid for consolidated rocks that do not deform or have an insignificant deformation due to changes in the reservoir pore pressure, which is the case with conventional reservoirs. However, unconventional reservoirs such as shale are well known for being stress sensitive [19,20]. This means that the change in the reservoir pore pressure might lead to rock deformation, affecting the fluid flow in the reservoir. For example, the reservoir pore pressure is reduced due to fluid production. The reduction in the reservoir pore pressure increases the effective stress. The increment in the effective stress would lead to rock compaction, which will eventually reduce the permeability. The permeability reduction will change the fluid flow in the reservoir. Consequently, coupling fluid flow with geomechanics in reservoir simulators should be considered for more accurate modeling.

The coupling of geomechanics with fluid flow in porous media can be achieved by applying consolidation theories in reservoir rocks. Terzaghi [21,22] was the first to introduce the idea of effective stress in consolidation, which provided a framework for fluid and rock interaction. In addition, Biot's theory of poroelasticity is the most widely used theory to explain the poromechanical interaction [23-25]. Biot's theory is a mathematical model describing the deformation of a porous medium saturated with fluid. Greetingsma [26] was the first to present a unified treatment of rock mechanics in petroleum production engineering. Geomechanics coupling with the fluid flow is important in any numerical modeling affected by poroelasticity, such as CO₂ or H₂ underground storage [27-29].

The fluid flow coupling with geomechanics has gained significant attention lately. The effect of mechanical rock properties and hydraulic fracture geometry on fluid flow has been studied extensively [19,30-38]. However, when using such a numerical approach, the effect of the reservoir matrix petrophysical parameters is under-investigated. As a result, this paper aims to study the effect of reservoir matrix permeability on the production performance of a gas-producing horizontal well completed with multistage hydraulic fracturing. In addition, this paper aims to show the difference between the cases when the geomechanics effects are coupled with the reservoir simulator and when it is decoupled.

2. Methodology

The present study utilizes a model that fully couples the fluid flow in porous media with geomechanics. The fluid flow model is governed by mass balance (i.e., continuity equation) and assumes a single-phase fluid flow that follows the Darcy law throughout the domain. In addition, the geomechanical deformation is governed by the equilibrium equation. The coupled model assumes the system is isothermal; hence, the temperature will not influence the flow in the model.

2.1 Governing Equations

For a transient flow, the continuity equation for a single-phase gas flow that considers the rock deformation rate is given

$$\frac{\partial}{\partial t}(\phi \rho_g) + \nabla \cdot (\phi \rho_g (\vec{v}_{gs} + \vec{v}_s)) = \rho_g q_g \quad (1)$$

where ϕ is the porosity, ρ_g is the gas density, \vec{v}_{gs} is the gas interstitial velocity, \vec{v}_s is the deformation rate of the solid phase (rock) due to flow in porous media, and q_g is the sink/source term. On the right-hand side of Eq. (1), the first term is the accumulation, and the second is the fluxes. The left-hand side of Eq. (1) is the sink/source term.

Based on Biot and Willis [23] and Geertsma [26] consolidation theory, the coupling between bulk volume and pore volume can be described through the porosity time derivative

$$\frac{\partial \phi}{\partial t} = \frac{b - \phi}{K_s} \frac{\partial P}{\partial t} + (b - \phi) \frac{\partial \varepsilon_v}{\partial t} \quad (2)$$

where b is Biot's coefficient, K_s is the solid grain stiffness (the solid grain bulk modulus), P is the pore pressure, ε_v is the volumetric strain.

Using the chain rule, the time derivative of the fluid density is expressed by

$$\frac{\partial \rho_g}{\partial t} = \frac{\partial \rho_g}{\partial P} \frac{\partial P}{\partial t} = \rho_g c_g \frac{\partial P}{\partial t} \quad (3)$$

where c_g is the gas compressibility.

In the continuity Eq. (1), assuming viscous flow and Darcy flow [19], Darcy's law is used in the calculation of the gas flux term [39]. Darcy's law can be described through the gas interstitial velocity as

$$\vec{v}_g = \phi \vec{v}_{gs} = \frac{\mathbf{k}}{\mu_g} \cdot [-\nabla P + \rho_g \vec{g}] \quad (4)$$

where \mathbf{k} is the second-order permeability tensor, μ_g is the gas viscosity and \vec{g} is the gravitational acceleration vector. In this study, the permeability is assumed to be isotropic as a result a single permeability value is used.

The deformation rate of the solid phase (rock) due to flow in porous media is equal to the displacement time derivative

$$\vec{v}_s = \frac{\partial \vec{u}}{\partial t} \quad (5)$$

where \vec{u} is the solid displacement.

Using small strain approximation, the volumetric strain ε_v is given by

$$\varepsilon_v = \nabla \cdot \vec{u} \quad (6)$$

Substituting Eq. (2), (3), (4), (5), and (6) to Eq. (1), and assuming infinitesimal deformation, Eq. (1) becomes

$$\rho_g \left(\frac{b-\phi}{K_s} \frac{\partial P}{\partial t} + (b-\phi) \frac{\partial \varepsilon_v}{\partial t} \right) + \phi \rho_g c_g \frac{\partial P}{\partial t} + \nabla \cdot (\rho_g \vec{v}_g) + \phi \rho_g \frac{\partial \varepsilon_v}{\partial t} = \rho_g q_g \quad (7)$$

Dividing by the gas density term and rearranging

$$\left(\frac{b-\phi}{K_s} + \phi c_g \right) \frac{\partial P}{\partial t} + b \frac{\partial \varepsilon_v}{\partial t} + \nabla \cdot (\vec{v}_g) = q_g \quad (8)$$

Eq. (8) is the governing equation of the model's pressure diffusion (continuity equation) governing the mass balance. Usually, conventional reservoir simulators approximate the velocity field using the multipoint flux approximation (MPFA) method, in which the velocity field can be approximated using the pressure difference between the connected cells. However, the model used in this study treats the velocity as a primary variable, which leads to higher local accuracy of the velocity field [32,40]. Eq. (4) is the velocity governing equation, which governs the flow in the porous media in the model used in this study.

The equation that governs the rock deformation assuming linear elasticity can be expressed by the Equilibrium equation

$$\nabla \cdot \sigma + \rho_b \vec{g} = 0 \quad (9)$$

where σ is the stress tensor, ρ_b is the bulk density.

The bulk density is given by

$$\rho_b = \phi \rho_g + (1-\phi) \rho_m \quad (10)$$

where ρ_m is the rock matrix density.

Following the typical geomechanics convention, the compressive stresses are denoted as positive [41,42], thus the stress tensor is expressed by

$$\sigma = \sigma_0 - \sigma' + b(P - P_0) \mathbf{I} + \rho_b \vec{g} \quad (11)$$

where σ_0 is the initial stress tensor, σ' is the effective stress, P_0 is the initial total pressure and \mathbf{I} is the second rank identity tensor.

For isotropic material, the effective stress is given by

$$\sigma' = 2G\varepsilon + \lambda\varepsilon_v \mathbf{I} \quad (12)$$

where ε is the strain tensor, G is the shear modulus and λ is the first Lamé parameter.

The shear modulus and first Lamé parameter are given in Eq. (13) and (14), respectively

$$G = \frac{E}{2(1+\nu)} \quad (13)$$

$$\lambda = \frac{E\nu}{(1+\nu)(1-2\nu)} \quad (14)$$

where E is Young's modulus and ν is Poisson's ratio.

The strain is related to the solid displacement using the expression

$$\varepsilon = \frac{1}{2} \left(\nabla \vec{u} + (\nabla \vec{u})^T \right) \quad (15)$$

Eq. (11) is the governing equation for the geomechanical deformation.

Eq. (8), (4) and (11) are the three governing equations that solve for the pore pressure P , gas velocity \vec{v}_g , and rock displacement \vec{u} .

2.2 Numerical Approach

The three governing equations solve for three unknowns: pore pressure P_h , gas velocity \vec{v}_h , and solid displacement \vec{u}_h . These three variables are interpolated using the mixed finite element scheme. The function spaces used to solve the three governing equations are the Discontinuous Galerkin (DG), the Raviart-Thomas (RT), and the Continuous Galerkin (CG) for the pressure diffusion equation, the gas velocity equation, and the solid displacement equation, respectively. The combination of finite element types for these function spaces has been selected because their solution has shown to be stable [32,43-46].

The governing equations' weak form was derived using the traditional Galerkin method. Three test functions were used to derive the weak form equations: P_t , \vec{V}_t , and \vec{U}_t . Multiplying Eq. (8), (4), and (11) by the test functions P_t , \vec{V}_t , and \vec{U}_t , respectively, integrating over the domain Ω and rearranging results into the final weak form of the governing equations

$$\int_{\Omega} \left[\frac{b - \phi^{n+1,m}}{K_s} + \phi^{n+1,m} c_g \right] \frac{P^{n+1,m+1} - P^n}{\Delta t} P_t d\Omega + \int_{\Omega} b \frac{\varepsilon_v^{n+1,m+1} - \varepsilon_v^n}{\Delta t} P_t d\Omega + \int_{\Omega} \nabla \cdot \vec{v}_g^{n+1,m+1} P_t d\Omega = \int_{\Omega} q_g^{n+1,m} P_t d\Omega \quad (16)$$

$$\int_{\Omega} \frac{\mu_g}{k^{n+1,m}} \vec{v}_g^{n+1,m+1} \cdot \vec{V}_t d\Omega = \int_{\Omega} P^{n+1,m+1} \nabla \cdot \vec{V}_t d\Omega - \int_{\Gamma} P^{n+1,BC} n \cdot \vec{V}_t d\Gamma + \int_{\Omega} \rho_g \vec{g} \cdot \vec{V}_t d\Omega \quad (17)$$

$$\int_{\Omega} \sigma_0 \cdot \varepsilon(\vec{U}_t) d\Omega - \int_{\Omega} 2G\varepsilon(\vec{u}^{n+1,m+1}) \cdot \varepsilon(\vec{U}_t) d\Omega - \int_{\Omega} \left(\nabla \cdot \vec{u}^{n+1,m+1} \right) \cdot \lambda (\nabla \cdot \vec{U}_t) d\Omega + \int_{\Omega} b (P^{n+1,m+1}) \cdot (\nabla \cdot \vec{U}_t) d\Omega - \int_{\Omega} b (P_0) \cdot (\nabla \cdot \vec{U}_t) d\Omega + \int_{\Omega} \rho_b^{n+1,m} \vec{g} \cdot \vec{U}_t d\Omega = \int_{\Gamma} (\mathbf{t}^{n+1,BC} \cdot \mathbf{n}) \cdot \vec{U}_t d\Gamma \quad (18)$$

where the superscripts n and $n+1$ are the previous time step and the current time step, respectively, the superscripts m and $m+1$ are the previous Picard iteration and the current Picard iteration, respectively, $P^{n+1, BC}$ is the stipulated pressure boundary condition, and $t^{n+1, BC}$ is the stipulated traction boundary condition.

As a result of gas production, the pore pressure is reduced, thus altering the effective stress, which leads to rock deformation. Consequently, the porosity and permeability are altered [47-51]. When the solid displacement and pore pressure solutions are obtained, the porosity is updated using Biot and Willis [23] and Geertsma [26] consolidation theory. Similarly, the permeability is updated using the exponential porosity-dependent permeability developed by Davies and Davies [52].

The initial conditions for the three unknowns are as below

$$P_0 = P_i \tag{19}$$

$$\vec{v}_0 = 0 \tag{20}$$

$$\vec{u}_0 = 0 \tag{21}$$

where P_0 is the pore pressure initial condition, P_i is the initial pore pressure, \vec{v}_0 is the initial gas velocity, and \vec{u}_0 is the initial rock displacement. The flow rate and the rock displacement are assumed to be zero at the beginning of the simulation. The six boundaries shown in Figure 1 are no flow boundaries. In addition, the vertical stress S_v is applied at the top boundary as a constant traction t and the other five boundaries are fixed with zero displacements. The sink/source term is defined using the Peaceman equation [53]. The wells are constrained by a constant bottomhole pressure in the sink/source term. It is important to note that the pressure and traction boundary conditions are applied as Neumann boundary conditions, while the total velocity and displacement boundary conditions are applied as Dirichlet boundary conditions. Figure 1 shows the model schematics used in this study. It shows a single well in the middle of the domain with six discrete hydraulic fractures and a stimulated rock volume (SRV) that numerically represents the enhanced permeability caused by the propagation of the fissures around the hydraulic fractures.

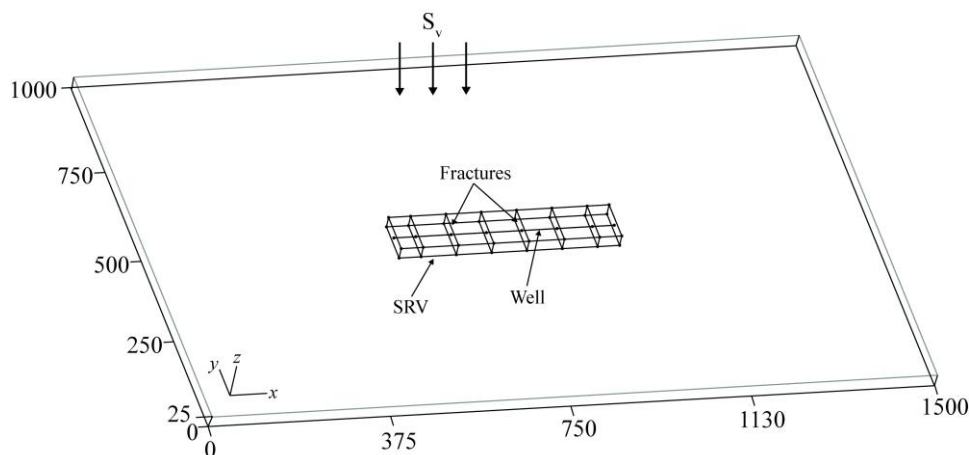


Fig. 1. Schematic of the model dimensions that highlights the SRV, the fractures and the well

The time derivative is discretized with a backward Euler scheme. The Picard iterations are employed to handle the model's non-linearity (e.g., porosity and permeability). FEniCS Project is used

to solve the system of the partial differential equations of the fluid flow coupling with geomechanics [54]. FEniCS Project is an open-source Finite Element library with high-level Python and C++ interfaces. FEniCS Project uses several advances in automated finite element methodologies, including but not limited to DOLFIN [55], FIAT [56], FFC [57], and UFL [58]. PETSc is the default linear algebra backend for FEniCS Project [59]. For the model used in this study, the weak form equations were coded in Unified Form Language (UFL), while the rest of the model dependencies were coded using Python. The code used in this study is an extension of the code provided in [46]. FEniCS Project can automatically handle mesh generation, function spaces, and finite element assembly and solution. One of the features that the FEniCS Project offers is the use of internal MPI commands that allow for parallel computation [60]. Consequently, the code, including the Picard iterations, can be run in multiple processors, which helps in reducing the computation time significantly.

Eq. (16) through (18) are solved monolithically in a mixed finite element scheme. This approach avoids numerical dispersion and unphysical oscillations in the pressure and displacement solutions [44]. Although the monolithic approach (fully coupling) complicates the numerical method by solving long equations, this method can achieve high solution stability and convergence compared to the staggered model (sequential coupling) [61-63]. Additionally, FEniCS Project can automatically handle the complications produced by the monolithic approach [46]. The validation of the numerical method used in this study against Terzaghi's one dimensional consolidation theoretical solution has been shown in a previous work of ours [64].

2.3 Data

This study uses data from Barnett Shale to construct the reservoir model. The input used in this study is based on fluid, reservoir, and production data that are available from the literature; Song *et al.*, [65] and Gou *et al.*, [32]. The geomechanics data for the model is based on data from Vermilyen [66], Yu and Sepehrnoori [67], and Zoback [42]. The detailed model data are presented in Table 1. Figure 1 shows the model dimensions of the multistage discrete hydraulic fractures that are used to investigate the performance of the horizontal well. Data in Table 1 is used to match the production history, as shown in Figure 2.

Table 1
 Fluid, reservoir, and rock parameters for history matching

Parameter(s)	Value(s)	Unit
Initial reservoir pressure	26.9 (3901.5)	MPa (Psi)
Bottom hole pressure	3.4 (493.13)	MPa (Psi)
Gas Viscosity	2.01×10^{-5} (0.02)	Pa.s (cP)
Matrix permeability	9.87×10^{-19} (1)	m^2 (μD)
Permeability of SRV	4.93×10^{-17} (50)	m^2 (μD)
Matrix porosity	15	%
Porosity of SRV	6.5	%
Fracture conductivity	1.35×10^{-15} (4.5)	m^2 -m (md-ft)
Fracture half-length	46 (151)	m (ft)
Fracture Spacing	73 (239.5)	m (ft)
Fracture stages	6	-
Rock matrix density	2.58×10^3 (161.1)	Kg/m^3 (lb/ft ³)
Biot's coefficient	1	-
Young's modulus	40 (5.8×10^6)	GPa (Psi)
Poisson's ratio	0.25	-
Vertical Stress	44 (6381.6)	MPa (Psi)
Maximum horizontal stress	29 (4206)	MPa (Psi)
Minimum horizontal stress	28 (4061)	MPa (Psi)

3. Results and Discussion

3.1 History Matching

In Figure 2, the y-axis represents the gas flow rate at reservoir conditions, while the x-axis represents the production time. Figure 2 shows the history-matching results; the circles represent the data gathered from a gas-producing well in Barnett Shale [65]. The numerical results when the geomechanical effects were decoupled from the reservoir simulators and constant rock compressibility was used instead are represented by the dotted line. At the same time, the numerical results when the geomechanical effects were coupled with the reservoir simulator are represented by the solid line. The production data gathered from the field seem noisy due to unknown production conditions. However, the field data exhibits a clear production profile because a constant bottomhole pressure was used throughout the simulation. The numerical models (coupled and decoupled) match the production profile of the filed production data. While the decoupled numerical model appears to overestimate the production flow rate compared to the field production data, the coupled numerical model matches the field production data more accurately. The numerical analysis is carried out accordingly since the history matching has been achieved.

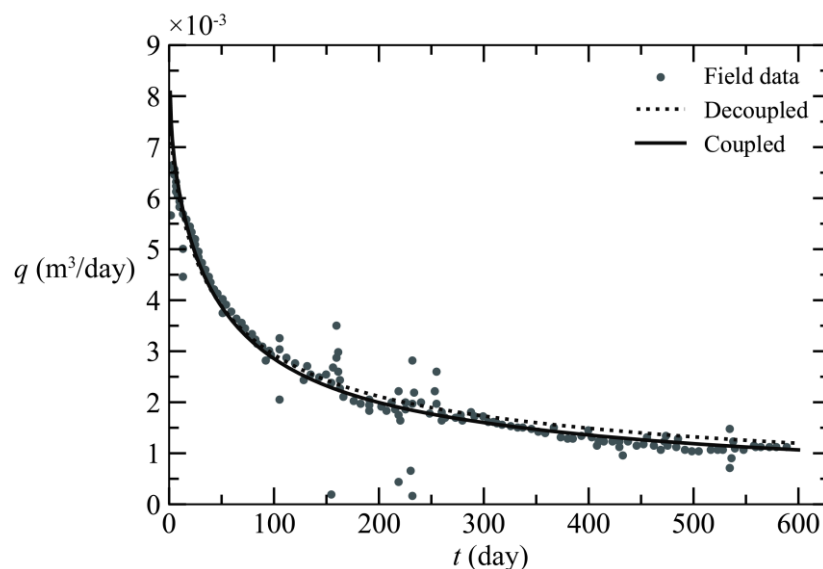


Fig. 2. History matching of the numerical model (coupled and decoupled) with the field data

3.2 Production History

Figure 3(a) shows a comparison of the reservoir production flow rate between the coupled (solid line) and the decoupled (dotted line) cases. In Figure 3(a), the x-axis represents the time, and the y-axis represents the reservoir production flow rate. After achieving history matching with field data, the production was extended to 5.1 years, as shown in Figure 3(a). The flow rate resulting from the coupled and the decoupled numerical cases appears to be the same in the first 6 months of production. However, after 6 months of production, there seems to be a slight difference between the coupled and the decoupled cases in the production profile. This difference is due to the consideration of rock deformation in the coupled case. As mentioned in the former sections, the pore pressure is reduced due to production, increasing the effective stress [42,68]. The increment in the effective stress results in rock compaction, thus reducing the porosity and permeability. This reduction in porosity and permeability is reflected by the slight reduction in the flow rate when the

geomechanical effects were coupled. In Figure 3(a), the difference in flow rate between the coupled and the decoupled cases does not seem significant.

Figure 3(b) shows the cumulative production (N_p) for 5.1 years for the coupled and the decoupled cases. In Figure 3(b), the x-axis represents the time, while the y-axis represents the cumulative production. While the difference in production flow rate was insignificant, as shown in Figure 3(a), the cumulative production estimation resulting from the coupled and the decoupled cases seem to be more notable, as shown in Figure 3(b). When the geomechanical effects were decoupled, the reservoir simulator overestimated the cumulative production by 7.9% compared to when the geomechanical effects were coupled.

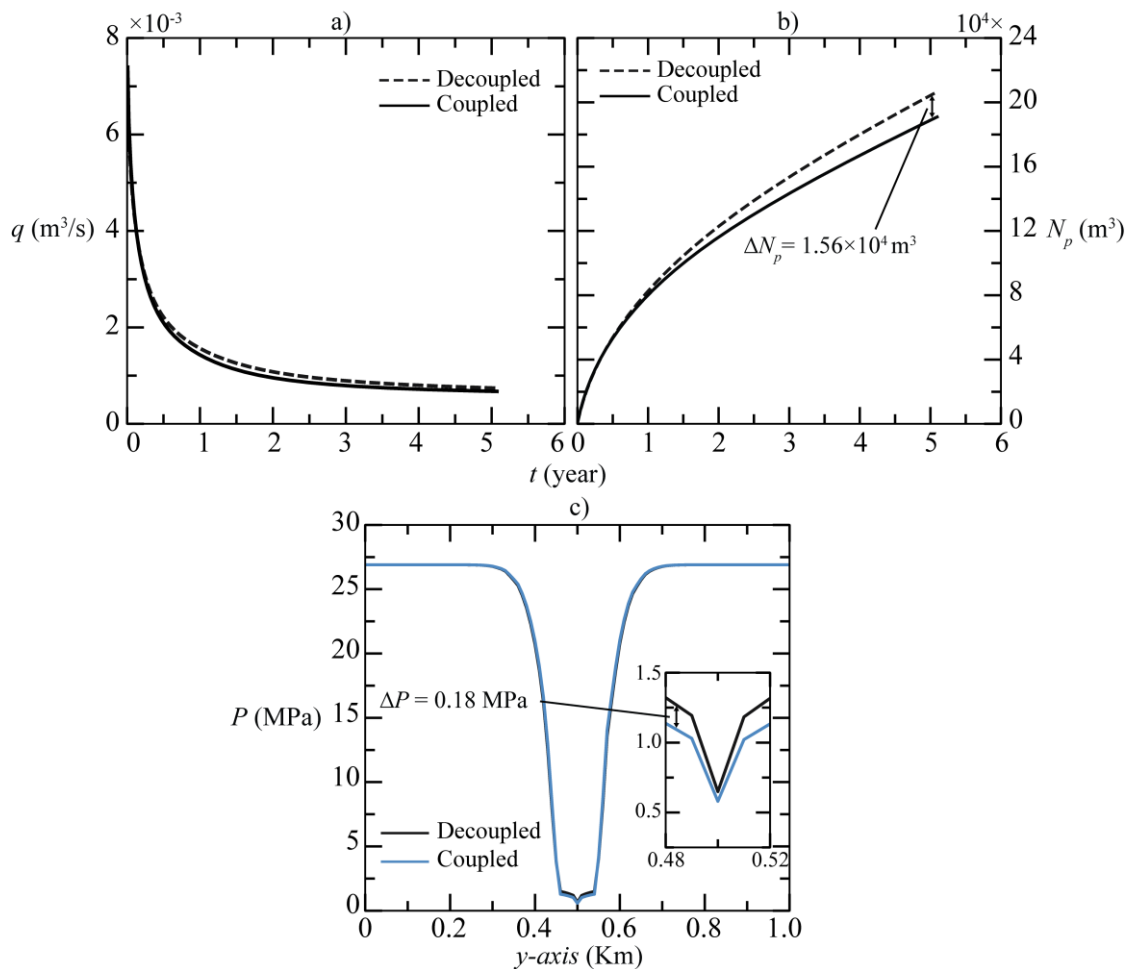


Fig. 3. (a) Flow rate for the coupled vs. decoupled cases, (b) a comparison of the cumulative production between the coupled and the decoupled cases, and (c) a comparison of the pore pressure along the third fracture between the coupled and the decoupled cases

Figure 3(c) shows the pore pressure along the third fracture along a 1-dimensional line extended in the y direction. The pressure depletion along the third and fourth fractures seems higher than the other fractures, as shown in Figure 4. As a result, the third fracture was chosen for data collection to investigate the pore pressure depletion differences between the coupled and the decoupled cases. In Figure 3(c), the pore pressure for the coupled and the decoupled cases are the same along the third fracture. However, there appears to be a slight difference in the middle of the domain, where the well is placed. The pore pressure depletion in the coupled case is higher than that of the decoupled case. It is expected that due to the lower flow rate in the coupled case, the pore pressure

would be higher than that of the decoupled case, as shown in Figure 3(a) and 3(b); however, the pore pressure profile shows the opposite behavior. This was a direct result of the rock deformation in the coupled case, which reduced the porosity and permeability, resulting in a rapid depletion of the pore pressure.

Figure 4(a) and 4(a*) show a planer top view of the pore pressure contour after 5.1 years of production for the decoupled and coupled numerical cases, respectively. The pressure contours shown in Figure 4(a) and 4(a*) are cropped from the original model shown in Figure 1 because significant pore pressure depletion occurred mostly within the SRV area, as also shown in Figure 3(c). Both coupled and decoupled cases show the pore pressure depletion propagation in the domain in a ripple effect manner. Notably, the pore pressure reduction along the six fractures seems more prominent than the rest of the SRV area and the reservoir matrix. Generally, the pore pressure contours show a more significant pore pressure depletion when the geomechanical effects were coupled with the reservoir simulator.

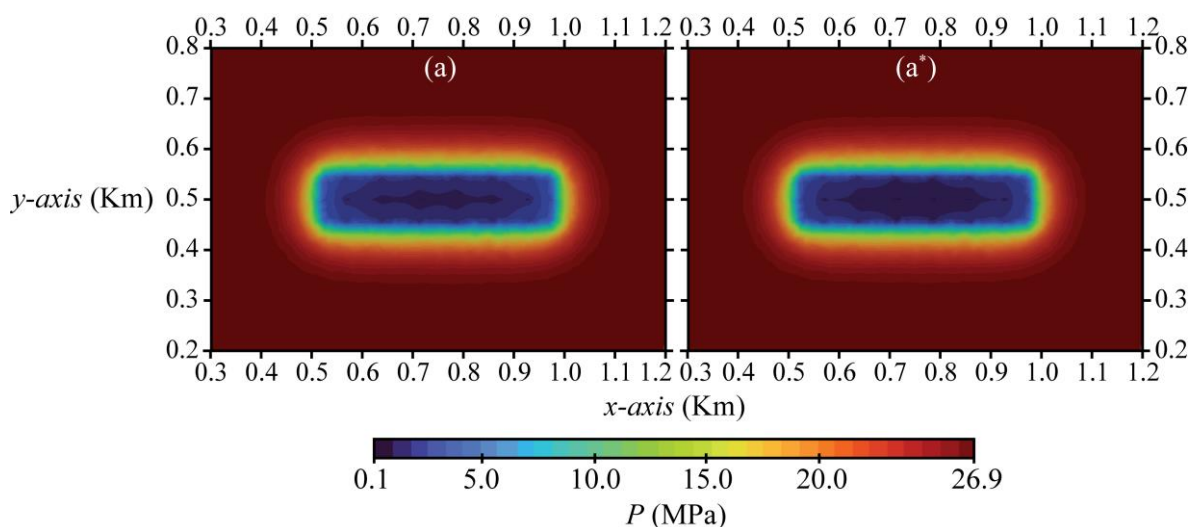


Fig. 4. Pore pressure contour for (a) the decoupled case and (a*) the coupled case

3.3 Sensitivity Analysis

After the production profile for the decoupled and coupled base cases was shown, this section aimed to show the sensitivity analysis. The sensitivity analysis carried out in this study investigates the matrix permeability. The varied parameters used for the sensitivity analysis are within the range of the typical shale rock parameters [69,70]. The aim is to study the differences in production estimation performance between the decoupled and the coupled cases. Table 2 shows the varied parameters used in this study.

Table 1
 Fluid, reservoir, and rock parameters for history matching

Parameter	Base case	$k m^2 (\mu D)$
$k m^2 (\mu D)$	9.87×10^{-19} (1.0)	9.87×10^{-20} (0.1)
		1.88×10^{-18} (1.9)

Figure 5 shows the sensitivity analysis for the matrix permeability. It shows the cumulative production volume comparison between the coupled and decoupled cases for low and high matrix permeabilities, as shown in Figure 5(a) and 5(b). In Figure 5(a) and 5(b), the x-axis represents the

time, while the y-axis represents the cumulative gas production volume. Figure 5 also shows the pore pressure along the third fracture at the end of simulation time (5.1 years) comparison between the coupled and decoupled cases for low and high matrix permeabilities, as shown in Figures 5(c) and 5(d), respectively. In Figure 5(c) and 5(d), the x-axis represents the distance along the y-axis, while the y-axis represents the pore pressure at the end of simulation time (5.1 years).

In Figure 5(a), the solid lines represent the base cases for the coupled and decoupled simulations, similar to those shown in Figure 3(b). The dotted lines represent the varied matrix permeability at $0.1 \mu\text{D}$. Figure 5(a) shows that the horizontal well production performance was affected adversely as the matrix permeability is reduced. Figure 5(a) also shows that as the matrix permeability was reduced, the difference between the coupled and the decoupled cases was about half of the base cases. However, the decoupled cases of the low matrix permeability still overestimate the gas cumulative production volume. Figure 5(c) shows the pore pressure along the third fracture, corresponding to the case shown in Figure 5(a). In Figure 5(c), the solid lines represent the base cases for the coupled and decoupled cases, while the dotted lines represent the varied matrix permeability at $0.1 \mu\text{D}$. Figure 5(c), 6(a), and 6(a*) show that as the matrix permeability was reduced, the extension of the pore pressure reduction from the SRV was less than that of the base cases. Figure 5(c) also shows that the pore pressure at the center of the fracture (at the well) is lower in the low permeability case compared to the base case in both the coupled and the decoupled cases. In addition, the difference in pore pressure estimation at the center of the third fracture between the coupled and decoupled cases for the low matrix permeability is about half that of the base cases. Results from Figure 5(a) and 5(c) show that the difference between coupled and decoupled cases is also reduced as the matrix permeability is reduced.

Similar to Figure 5(a) and 3(b), the solid lines in Figure 5(b) represent the gas cumulative production volume for the coupled and decoupled base cases. In Figure 5(b), the dotted lines represent the coupled and decoupled cases at the matrix permeability of $1.9 \mu\text{D}$, which is the high permeability case. The estimated gas cumulative production volume is higher than the base cases for both the coupled and decoupled cases at high matrix permeability, as shown in Figure 5(b). In Figure 5(b), the decoupled case overestimates the gas cumulative production volume, which is the same trend as in Figure 5(a) and 3(b). In addition, the difference between the coupled and the decoupled cases in the high matrix permeability scenario is higher than that of the base cases. Figure 5(d) shows the pore pressure along the third fracture for the case corresponding to the one shown in Figure 5(b). It appears that as the matrix permeability is increased, the pore pressure reduction extends away from the SRV further than that of the base cases, as shown in Figure 5(d), 6(b), and 6(b*). Figure 5(d) also shows that at the center of the third fracture, the pore pressure at the high permeability case was higher than that of the base case at the end of the simulation time (5.1 years). In addition, the difference between the pore pressure at the center of the third fracture between the coupled and the decoupled cases at high matrix permeability is higher than that of the base cases. This shows that as the matrix permeability gets higher, the decoupled model seems to further overestimate the gas cumulative production volume compared to the lower matrix permeability.

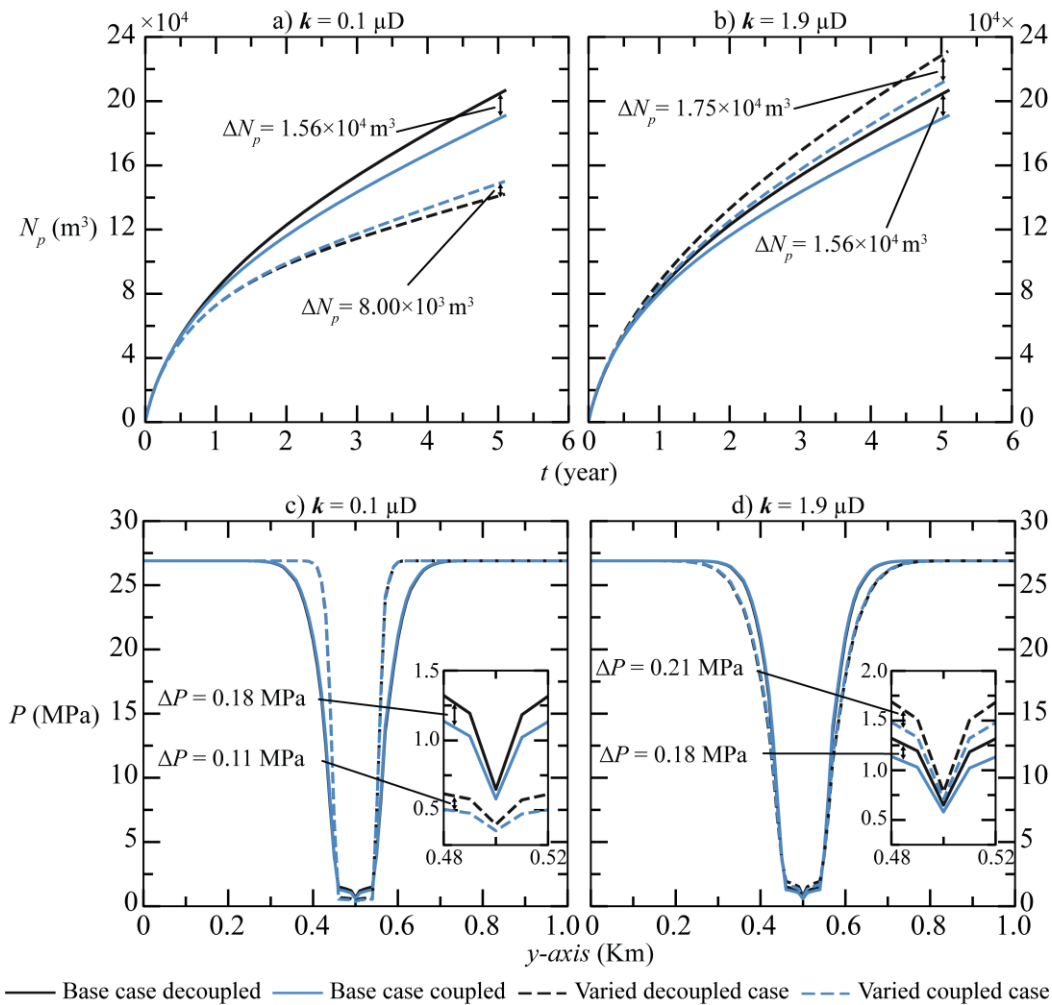


Fig. 5. Matrix permeability sensitivity analysis comparison between coupled and decoupled cases for (a) cumulative production for the low permeability, (b) cumulative production for the high permeability, (c) the pore pressure along the third fracture for the low permeability case, (d) the pore pressure along the third fracture for the high permeability case

Figure 6 shows the pore pressure contours of the sensitivity analysis carried out in this study. Figure 6(a) and 6(b) show the pore pressure contours of the decoupled low and high matrix permeability cases, respectively. Figure 6(a*) and 6(b*) show the pore pressure contours of the coupled low and high permeability cases, respectively. Figure 6 shows that at low matrix permeability, the pore pressure reduction extension beyond the SRV is limited, as shown in Figure 6(a) and 6(a*). Inversely, at high matrix permeability, the pore pressure contours in Figures 6(b) and 6(b*), the pore pressure reduction extends beyond the SRV. This explains the increased gas cumulative production volume at the high matrix permeability cases. From Figure 6, it can also be noted that the pore pressure reduction inside the SRV is greater at the low matrix permeability cases, as shown in Figure 6(a) and 6(a*). Consequently, the gas was greatly depleted in the SRV when the matrix permeability was low.

In Figure 6, for both the low and high matrix permeability cases, the pore pressure contours show that the pore pressure reduction in coupled cases is greater than that of the decoupled cases. The reason for that is the consideration of the rock deformation in the coupled cases. According to Biot's theory, the effective stress increases as the pore pressure reduces [22-24]. The increment in the effective stress alters the porosity, affecting the permeability. Consequently, the pore pressure

contours show that the pore pressure reduction in the coupled cases seems slightly higher than that of decoupled cases. The permeability reduction due to rock deformation led to this greater reduction in the pore pressure in the coupled cases, resulting in a less gas cumulative production volume estimation.

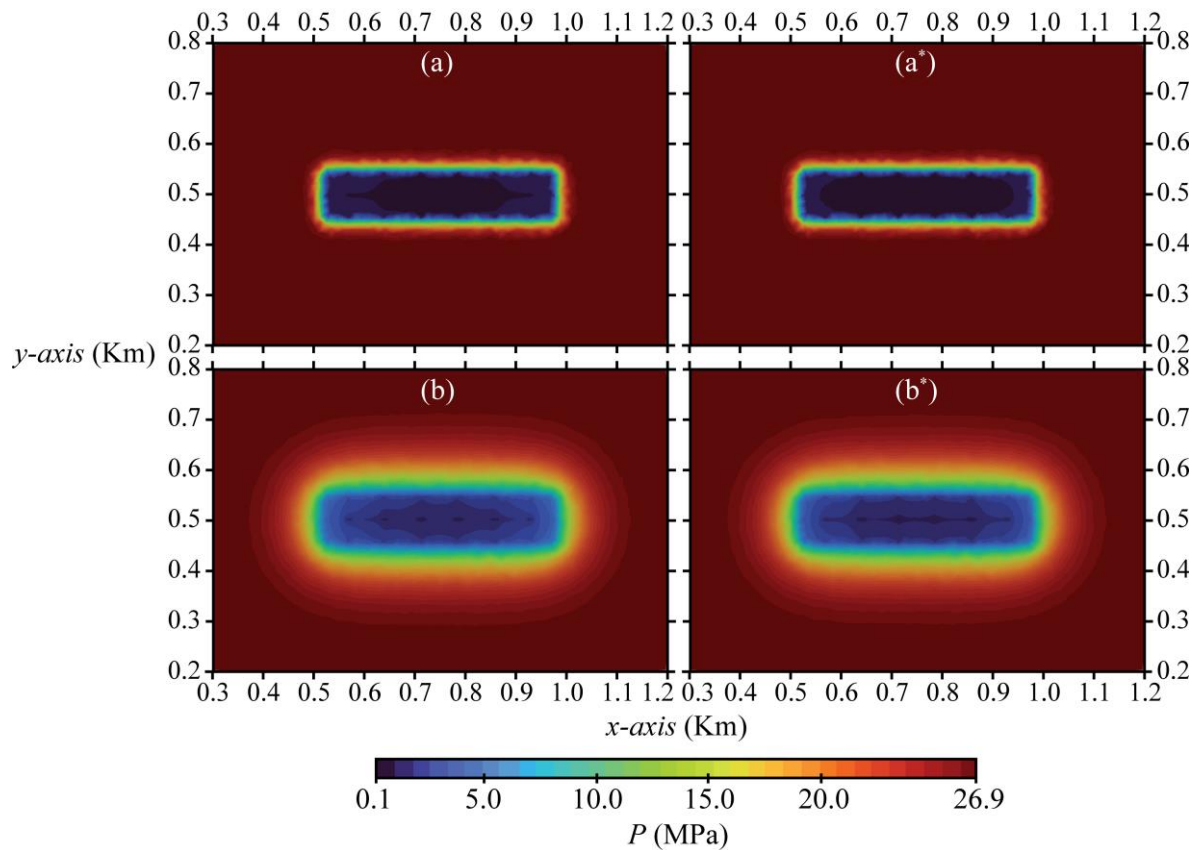


Fig. 6. Pressure contours of matrix permeability sensitivity analysis for (a) the low permeability decoupled case and (a*) the low permeability coupled case, (b) the high permeability decoupled case, and (b*) the high permeability coupled case

4. Conclusions

The utilization of conventional modeling techniques to numerically study hydrocarbon extraction from unconventional resources can lead to inaccurate production estimations. The unconventional hydrocarbon resources are commonly found in shale rock formations. The shale rock formations are well-known for being stress-sensitive. The conventional modeling techniques use a constant value to denote rock deformation. However, for stress-sensitive formation, the mechanical parameters of the rock must be considered for modeling the hydrocarbon extraction from unconventional resources. This paper used a fully coupled fluid flow with a geomechanics model to study hydrocarbon production from Barnett Shale. Usually, when such an approach is utilized to study the hydrocarbon production from shale formations, the petrophysical properties, such as the matrix permeability, are rarely studied. This paper studied the effect of matrix permeability on the production performance of a single horizontal well when the geomechanics effect was coupled and decoupled with the fluid flow model. This study showed the difference in production estimation between the cases when the geomechanics effect was coupled with the fluid flow model and decoupled. The summary of findings from this study is as follows:

- i. When the matrix permeability was increased, the gas cumulative production volume estimation also increased in the coupled and decoupled cases. In addition, low matrix permeability led to a greater pore pressure reduction in the Stimulated Rock Volume (SRV).
- ii. The decoupled model cases overestimated the gas cumulative production volume for both the high and low matrix permeabilities.
- iii. At low matrix permeability, the difference between the gas cumulative production volume between the coupled and decoupled cases was greatly reduced compared to the base case. This means that the decoupled model estimation of the gas cumulative production volume at lower matrix permeability was closer to that of the coupled model.
- iv. At high matrix permeability, the estimated gas cumulative production volume increased compared to the base cases. In addition, as the matrix permeability increased, the estimation difference between the coupled and decoupled cases in gas cumulative production volume also increased.
- v. In stress-sensitive formations such as shale formation, although most production occurs through hydraulic fractures, the matrix permeability still influences production. The conventional modeling technique's overestimation of the cumulative production increases as the matrix permeability increases.

Acknowledgement

The authors gratefully acknowledge financial support from the YUTP project at the Universiti Teknologi PETRONAS under Grant no. 015LC0-447.

References

- [1] Mikayilov, Jeyhun I., Shahriyar Mukhtarov, Hasan Dinçer, Serhat Yüksel, and Rıdvan Aydın. "Elasticity Analysis of Fossil Energy Sources for Sustainable Economies: A Case of Gasoline Consumption in Turkey." *Energies* 13 no. 3 (2020): 731. <https://doi.org/10.3390/en13030731>
- [2] Ovezmyradov, Berdymyrat, and Yolbars Kepbanov. "Dependence of Central Asian Countries on Fossil Energy and Low Adoption of Non-Hydro Renewables." Available at SSRN 4193407 (2022). <https://doi.org/10.2139/ssrn.4193407>
- [3] Abdullahi, M.B., S.R. Jufar, S. Kumar, T.M. Al-shami, and B.M Negash. "Synergistic Effect of Polymer-Augmented Low Salinity Flooding for Oil Recovery Efficiency in Illite-Sand Porous Media." *Journal of Molecular Liquids* 358 (2022): 119217. <https://doi.org/10.1016/j.molliq.2022.119217>
- [4] Caineng, Zou, Yang Zhi, Guosheng Zhang, Hou Lianhua, Zhu Rukai, Tao Shizhen, Yuan Xuanjun et al. "Conventional and unconventional petroleum "orderly accumulation": Concept and practical significance." *Petroleum Exploration and Development* 41, no. 1 (2014): 14-30. [https://doi.org/10.1016/S1876-3804\(14\)60002-1](https://doi.org/10.1016/S1876-3804(14)60002-1)
- [5] Muther, Temoor, Haris Ahmed Qureshi, Fahad Iqbal Syed, Hassan Aziz, Amaar Siyal, Amirmasoud Kalantari Dahaghi, and Shahin Negahban. "Unconventional Hydrocarbon Resources: Geological Statistics, Petrophysical Characterization, and Field Development Strategies." *Journal of Petroleum Exploration and Production Technology* 12, no.6 (2021):1463-1488. <https://doi.org/10.1007/s13202-021-01404-x>
- [6] Kampit, Stanley Jaul, Tuan Zaid Tuan Muda, Samira Albati Kamaruddin, Zulkarnain Abdullah Anas, and Mohd Nor Hisham Mohd Azam. "Heterolithic Thin Bedded Reservoirs Volumetric Estimation, Quantification and High-Resolution 3D Modelling." *Journal of Advanced Research in Applied Mechanics* 65, no. 1 (2020): 1-10. <https://doi.org/10.37934/aram.65.1.110>
- [7] Dhir, Ravindra K., Jorge de Brito, Raman Mangabhai, and Chao Qun Lye. "Use of copper slag in geotechnical applications." *Sustainable Construction Materials: Copper Slag*; Elsevier: Amsterdam, The Netherlands (2017): 211-245. <https://doi.org/10.1016/B978-0-08-100986-4.00006-7>
- [8] Abdulelah, Hesham, Berihun Mamo Negash, Nurudeen Yekeen, Sameer Al-Hajri, Eswaran Padmanabhan, and Ahmed Al-Yaseri. "Synergetic effect of surfactant concentration, salinity, and pressure on adsorbed methane in shale at low pressure: an experimental and modeling study." *ACS omega* 5, no. 32 (2020): 20107-20121.. <https://doi.org/10.1021/acsomega.0c01738>

- [9] Abdulelah, Hesham, Syed M. Mahmood, and Ahmed Al-Mutarreb. "Effect of anionic surfactant on wettability of shale and its implication on gas adsorption/desorption behavior." *Energy & Fuels* 32, no. 2 (2018): 1423-1432.. <https://doi.org/10.1021/acs.energyfuels.7b03476>
- [10] Ziarani, Ali S., Roberto Aguilera, and Albert X. Cui. "Permeability of tight sand and shale formations: a dual mechanism approach for micro and nanodarcy reservoirs." In *SPE Canada Unconventional Resources Conference?*, p. D033S003R002. SPE, 2020. <https://doi.org/10.2118/200010-MS>
- [11] Jia, Chengzao. "Breakthrough and significance of unconventional oil and gas to classical petroleum geology theory." *Petroleum Exploration and Development Online* 44, no. 1 (2017): 1-10. [https://doi.org/10.1016/S1876-3804\(17\)30002-2](https://doi.org/10.1016/S1876-3804(17)30002-2)
- [12] Fangzheng, J. I. A. O. "Re-recognition of "unconventional" in unconventional oil and gas." *Petroleum Exploration and Development* 46, no. 5 (2019): 847-855. [https://doi.org/10.1016/S1876-3804\(19\)60244-2](https://doi.org/10.1016/S1876-3804(19)60244-2)
- [13] Al-Shami, Tareq Mohammed, Shiferaw Regassa Jufar, Berihun Mamo Negash, and Mohammed Bashir Abdullahi. "Impact of External Excitation on Flow Behavior of Trapped Oil Blob." *Journal of Petroleum Science and Engineering* 196 (2021): 108002. <https://doi.org/10.1016/j.petrol.2020.108002>
- [14] Al-Shami, Tareq Mohammed, Shiferaw Regassa Jufar, Berihun Mamo Negash, and Mohammed Bashir Abdullahi. "Impact of external excitation on flow behavior of trapped oil blob." *Journal of Petroleum Science and Engineering* 196 (2021): 108002. <https://doi.org/10.18178/ijmerr.8.6.998-1002>
- [15] Yang, Yun, and Shimin Liu. "Review of shale gas sorption and its models." *Energy & Fuels* 34, no. 12 (2020): 15502-15524. <https://doi.org/10.1021/acs.energyfuels.0c02906>
- [16] Lin, Wen. "A review on shale reservoirs as an unconventional play—the history, technology revolution, importance to oil and gas industry, and the development future." *Acta Geologica Sinica-English Edition* 90, no. 5 (2016): 1887-1902. <https://doi.org/10.1111/1755-6724.12823>
- [17] Abdulelah, Hesham, Berihun Mamo Negash, Tareq M. Al-Shami, Firas A. Abdulkareem, Eswaran Padmanabhan, and Ahmed Al-Yaseri. "Mechanism of CH₄ sorption onto a shale surface in the presence of cationic surfactant." *Energy & Fuels* 35, no. 9 (2021): 7943-7955. <https://doi.org/10.1021/acs.energyfuels.1c00613>
- [18] Al-Hajri, Sameer, Berihun M. Negash, Md Motiur Rahman, Mohammed Haroun, and Tareq M. Al-Shami. "Effect of Silica Nanoparticles on Polymer Adsorption Reduction on Marcellus Shale." *ACS omega* 6, no. 44 (2021): 29537-29546. <https://doi.org/10.1021/acsomega.1c03653>
- [19] Shovkun, Igor, and D. Nicolas Espinoza. "Coupled fluid flow-geomechanics simulation in stress-sensitive coal and shale reservoirs: Impact of desorption-induced stresses, shear failure, and fines migration." *Fuel* 195 (2017): 260-272. <https://doi.org/10.1016/j.fuel.2017.01.057>
- [20] Wei, Chenji, Liangang Wang, Baozhu Li, Lihui Xiong, Shuangshuang Liu, Jie Zheng, Suming Hu, and Hongqing Song. "A study of nonlinear elasticity effects on permeability of stress sensitive shale rocks using an improved coupled flow and geomechanics model: a case study of the Longmaxi shale in China." *Energies* 11, no. 2 (2018): 329. <https://doi.org/10.3390/en11020329>
- [21] Terzaghi, K. "Die Berechnung Der Durchlässigkeitsziffer Des Tones Aus Dem Verlauf Der Hydrodynamischen Spannungerscheinungen Akademie Der Wissenschaften." *Akademie Der Wissenschaften in Wien. Sitzungsberichte* 11 (1923): 105–24. <https://doi.org/10.1007/BF01551781>
- [22] Terzaghi, K. "Erdbaumechanik auf bodenphysikalischer Grundlage (Mechanics of earthworks based on rudiments of soil physics)." *Deuticke* (1925).
- [23] Biot, Maurice A., and David G. Willis. "The elastic coefficients of the theory of consolidation." (1957): 594-601. <https://doi.org/10.1115/1.4011606>
- [24] Biot, Maurice A. "Theory of elasticity and consolidation for a porous anisotropic solid." *Journal of applied physics* 26, no. 2 (1955): 182-185. <https://doi.org/10.1063/1.1721956>
- [25] Biot, Maurice A. "General theory of three-dimensional consolidation." *Journal of applied physics* 12, no. 2 (1941): 155-164. <https://doi.org/10.1063/1.1712886>
- [26] Geertsma, J. "Problems of rock mechanics in petroleum production engineering." In *ISRM Congress*, pp. ISRM-1CONGRESS. ISRM, 1966.
- [27] Huang, Jian, and Ahmad Ghassemi. "A poroelastic model for evolution of fractured reservoirs during gas production." *Journal of Petroleum Science and Engineering* 135 (2015): 626-644. <https://doi.org/10.1016/j.petrol.2015.10.007>
- [28] Rutqvist, Jonny. "The geomechanics of CO₂ storage in deep sedimentary formations." *Geotechnical and Geological Engineering* 30 (2012): 525-551. <https://doi.org/10.1007/s10706-011-9491-0>
- [29] Elyasi1a, Ayub, Kamran Goshtasbi, and Hamid Hashemolhosseini. "A coupled geomechanical reservoir simulation analysis of CO₂-EOR: A case study." (2016). <https://doi.org/10.12989/gae.2016.10.4.423>
- [30] Chin, L. Y., and L. K. Thomas. "Fully coupled analysis of improved oil recovery by reservoir compaction." In *SPE Annual Technical Conference and Exhibition?*, pp. SPE-56753. SPE, 1999. <https://doi.org/10.2118/56753-MS>

- [31] Dean, Rick H., and Joseph H. Schmidt. "Hydraulic-fracture predictions with a fully coupled geomechanical reservoir simulator." *Spe Journal* 14, no. 04 (2009): 707-714. <https://doi.org/10.2118/116470-PA>
- [32] Guo, Xuyang, Hongqing Song, Kan Wu, and John Killough. "Pressure characteristics and performance of multi-stage fractured horizontal well in shale gas reservoirs with coupled flow and geomechanics." *Journal of Petroleum Science and Engineering* 163 (2018): 1-15. <https://doi.org/10.1016/j.petrol.2017.12.038>
- [33] Jiang, Jiamin, and Jie Yang. "Coupled fluid flow and geomechanics modeling of stress-sensitive production behavior in fractured shale gas reservoirs." *International Journal of Rock Mechanics and Mining Sciences* 101 (2018): 1-12. <https://doi.org/10.1016/j.ijrmms.2017.11.003>
- [34] Kim, Jihoon, G. J. Moridis, Daegil Yang, and Jonny Rutqvist. "Numerical studies on two-way coupled fluid flow and geomechanics in hydrate deposits." *SPE journal* 17, no. 02 (2012): 485-501. <https://doi.org/10.2118/141304-PA>
- [35] Liu, Yongzan, Lijun Liu, Juliana Y. Leung, and George J. Moridis. "Sequentially coupled flow and geomechanical simulation with a discrete fracture model for analyzing fracturing fluid recovery and distribution in fractured ultra-low permeability gas reservoirs." *Journal of Petroleum Science and Engineering* 189 (2020): 107042. <https://doi.org/10.1016/j.petrol.2020.107042>
- [36] Minkoff, Susan E., C. Mike Stone, Steve Bryant, Malgorzata Peszynska, and Mary F. Wheeler. "Coupled fluid flow and geomechanical deformation modeling." *Journal of Petroleum Science and Engineering* 38, no. 1-2 (2003): 37-56. [https://doi.org/10.1016/S0920-4105\(03\)00021-4](https://doi.org/10.1016/S0920-4105(03)00021-4)
- [37] Moradi, Mostafa, Amir Shamloo, and Alireza Danesh Dezfuli. "A sequential implicit discrete fracture model for three-dimensional coupled flow-geomechanics problems in naturally fractured porous media." *Journal of Petroleum Science and Engineering* 150 (2017): 312-322. <https://doi.org/10.1016/j.petrol.2016.12.027>
- [38] Yu, Wei, and K. Sepehrnoori. "Numerical evaluation of the impact of geomechanics on well performance in shale gas reservoirs." In *ARMA US Rock Mechanics/Geomechanics Symposium*, pp. ARMA-2013. ARMA, 2013. <https://doi.org/10.2118/167225-MS>
- [39] Hubbert, M. King. "Darcy's law and the field equations of the flow of underground fluids." *Hydrological Sciences Journal* 2, no. 1 (1957): 23-59. <https://doi.org/10.1080/02626665709493062>
- [40] Yang, Daegil. "A Simulator with numerical upscaling for the analysis of coupled multiphase flow and geomechanics in heterogeneous and deformable porous and fractured media." PhD diss., 2013.
- [41] Wood, David Muir. *Soil behaviour and critical state soil mechanics*. Cambridge university press, 1990. <https://doi.org/10.1017/CBO9781139878272>
- [42] Zoback, M. D. "Reservoir Geomechanics/Cambridge, New York, Melbourne: Cambridge University Press." (2007). <https://doi.org/10.1017/CBO9780511586477>
- [43] Zhang, Chao, Sadiq J. Zarrouk, and Rosalind Archer. "Development of a fully coupled flow-geomechanics simulator for flow in saturated porous media." In *The 6th International Conference on Computational Methods (ICCM2015)*. 2015.
- [44] Ferronato, Massimiliano, Nicola Castelletto, and Giuseppe Gambolati. "A fully coupled 3-D mixed finite element model of Biot consolidation." *Journal of Computational Physics* 229, no. 12 (2010): 4813-4830. <https://doi.org/10.1016/j.jcp.2010.03.018>
- [45] Yang, Daegil, George J. Moridis, and Thomas A. Blasingame. "A fully coupled multiphase flow and geomechanics solver for highly heterogeneous porous media." *Journal of Computational and Applied Mathematics* 270 (2014): 417-432. <https://doi.org/10.1016/j.cam.2013.12.029>
- [46] Haagensohn, Ryan, Harihar Rajaram, and Jeffery Allen. "A generalized poroelastic model using FEniCS with insights into the Noordbergum effect." *Computers & Geosciences* 135 (2020): 104399. <https://doi.org/10.1016/j.cageo.2019.104399>
- [47] Soeder, D. J., and P. L. Randolph. "Porosity, permeability, and pore structure of the tight Mesaverde Sandstone, Piceance Basin, Colorado." *SPE formation evaluation* 2, no. 02 (1987): 129-136. <https://doi.org/10.2118/13134-PA>
- [48] McKee, Chester R., Amar C. Bumb, and Robert A. Koenig. "Stress-dependent permeability and porosity of coal and other geologic formations." *SPE formation evaluation* 3, no. 01 (1988): 81-91. <https://doi.org/10.2118/12858-PA>
- [49] Geertsma, J. "The effect of fluid pressure decline on volumetric changes of porous rocks." *Transactions of the AIME* 210, no. 01 (1957): 331-340. <https://doi.org/10.2118/728-G>
- [50] Wei, K. K., N. R. Morrow, and K. R. Brower. "Effect of fluid, confining pressure, and temperature on absolute permeabilities of low-permeability sandstones." *SPE Formation Evaluation* 1, no. 04 (1986): 413-423. <https://doi.org/10.2118/13093-PA>
- [51] Dobrynin, Valery M. "Effect of overburden pressure on some properties of sandstones." *Society of Petroleum Engineers Journal* 2, no. 04 (1962): 360-366. <https://doi.org/10.2118/461-PA>
- [52] Davies, J. P., and D. K. Davies. "Stress-dependent permeability: characterization and modeling." *Spe Journal* 6, no. 02 (2001): 224-235. <https://doi.org/10.2118/56813-MS>

- [53] Peaceman, Donald W. "Interpretation of well-block pressures in numerical reservoir simulation (includes associated paper 6988)." *Society of Petroleum Engineers Journal* 18, no. 03 (1978): 183-194. <https://doi.org/10.2118/6893-PA>
- [54] Alnæs, Martin, Jan Blechta, Johan Hake, August Johansson, Benjamin Kehlet, Anders Logg, Chris Richardson, Johannes Ring, Marie E. Rognes, and Garth N. Wells. "The FEniCS project version 1.5." *Archive of numerical software* 3, no. 100 (2015). <https://doi.org/10.11588/ans.2015.100.20553>
- [55] Logg, Anders, and Garth N. Wells. "DOLFIN: Automated finite element computing." *ACM Transactions on Mathematical Software (TOMS)* 37, no. 2 (2010): 1-28. <https://doi.org/10.1145/1731022.1731030>
- [56] Kirby, Robert C. "Algorithm 839: FIAT, a new paradigm for computing finite element basis functions." *ACM Transactions on Mathematical Software (TOMS)* 30, no. 4 (2004): 502-516. <https://doi.org/10.1145/1039813.1039820>
- [57] Kirby, Robert C., and Anders Logg. "A compiler for variational forms." *ACM Transactions on Mathematical Software (TOMS)* 32, no. 3 (2006): 417-444. <https://doi.org/10.1145/1163641.1163644>
- [58] Alnæs, Martin S., Anders Logg, Kristian B. Ølgaard, Marie E. Rognes, and Garth N. Wells. "Unified form language: A domain-specific language for weak formulations of partial differential equations." *ACM Transactions on Mathematical Software (TOMS)* 40, no. 2 (2014): 1-37. <https://doi.org/10.1145/2566630>
- [59] Abhyankar, Shrirang, Jed Brown, Emil M. Constantinescu, Debojyoti Ghosh, Barry F. Smith, and Hong Zhang. "PETSc/TS: A modern scalable ODE/DAE solver library." *arXiv preprint arXiv:1806.01437* (2018). <https://doi.org/10.48550/arxiv.1806.01437>
- [60] Gabriel, Edgar, Graham E. Fagg, George Bosilca, Thara Angskun, Jack J. Dongarra, Jeffrey M. Squyres, Vishal Sahay et al. "Open MPI: Goals, concept, and design of a next generation MPI implementation." In *Recent Advances in Parallel Virtual Machine and Message Passing Interface: 11th European PVM/MPI Users' Group Meeting Budapest, Hungary, September 19-22, 2004. Proceedings 11*, pp. 97-104. Springer Berlin Heidelberg, 2004. https://doi.org/10.1007/978-3-540-30218-6_19
- [61] Kolesov, Alexandr E., Petr N. Vabishchevich, and Maria V. Vasilyeva. "Splitting schemes for poroelasticity and thermoelasticity problems." *Computers & Mathematics with Applications* 67, no. 12 (2014): 2185-2198. <https://doi.org/10.1016/j.camwa.2014.02.005>
- [62] Kim, Jihoon, Hamdi A. Tchelepi, and Ruben Juanes. "Stability and convergence of sequential methods for coupled flow and geomechanics: Fixed-stress and fixed-strain splits." *Computer Methods in Applied Mechanics and Engineering* 200, no. 13-16 (2011): 1591-1606. <https://doi.org/10.1016/j.cma.2010.12.022>
- [63] Al-Shami, Tareq Mohammed, Shiferaw Regassa Jufar, Sunil Kumar, Hesham Abdulelah, Mohammed Bashir Abdullahi, Sameer Al-Hajri, and Berihun Mamo Negash. "A comprehensive review of interwell interference in shale reservoirs." *Earth-Science Reviews* (2023): 104327. <https://doi.org/10.1016/j.earscirev.2023.104327>
- [64] Al-Shami, Tareq Mohammed, Shiferaw Regassa Jufar, Mohammed Bashir Abdullahi, and Berihun Mamo Negash. "A Study on the Production Performance of a Horizontal Shale Gas Well Using a Fully Coupled Flow and Geomechanics Modeling." *Journal of Advanced Research in Fluid Mechanics and Thermal Sciences* 105, no. 2 (2023): 146-165. <https://doi.org/10.37934/arfmts.105.2.146165>
- [65] Song, Hongqing, Zhengyi Li, Yuhe Wang, Weiyao Zhu, Yang Cao, and John Killough. "A novel approach for modeling gas flow behaviors in unconventional reservoirs with nanoporous media." In *International Petroleum Technology Conference*, p. D041S060R001. IPTC, 2015. <https://doi.org/10.2523/IPTC-18316-MS>
- [66] Vermynen, John Peter. *Geomechanical studies of the Barnett shale, Texas, USA*. Stanford University, 2011.
- [67] Yu, Wei, and Kamy Sepehrnoori. "Simulation of gas desorption and geomechanics effects for unconventional gas reservoirs." In *SPE Western Regional & AAPG Pacific Section Meeting 2013 Joint Technical Conference*. OnePetro, 2013. <https://doi.org/10.1016/j.fuel.2013.08.032>
- [68] Ajisafe, F. O., I. Solovyeva, A. Morales, E. Ejojodomi, and M. M. Porcu. *Impact of well spacing and interference on production performance in unconventional reservoirs, Permian basin. Unconventional Resources Technology Conference*. doi: 10.15530.URTEC-2017-2690466, 2017. <https://doi.org/10.15530/urtec-2017-2690466>
- [69] Guo, Chaohua, Mingzhen Wei, and Hong Liu. "Modeling of gas production from shale reservoirs considering multiple transport mechanisms." *PloS one* 10, no. 12 (2015): e0143649. <https://doi.org/10.1371/journal.pone.0143649>
- [70] Pei, Yanli, and Kamy Sepehrnoori. "Investigation of parent-well production induced stress interference in multilayer unconventional reservoirs." *Rock Mechanics and Rock Engineering* (2022): 1-22. <https://doi.org/10.1007/s00603-021-02719-1>